Fromreide, M., I. Monsen, J. O. Sundli, Ø. S. Sortland, U. Thisted, M. Sparta, and V. K. Risinggård. 2026. Modelling of neutral-point drift in a silicon furnace.
In Silicon for the chemical and solar industry XVIII, edited by M. Tangstad, H. Rong, A. Valderhaug, B. Andresen, H. Dalaker, and I. G. Page.
Kristiansand, Norway, September 7-10, 2026.
https://doi.org/10.55669/oa900802

Modelling of neutral-point drift in a silicon furnace

M. Fromreide[1], I. Monsen[1], J.O. Sundli[2], Ø.S. Sortland[1], U. Thisted[1], M. Sparta[1], V.K. Risinggård[1]
[1]NORCE Research AS, Norway, mafr@norceresearch.no
[2]Wacker Chemicals Norway AS, Norway

Keywords: Bøckman system, Neutral-point drift, Submerged Arc Furnace, Finite Element Model

Abstract – Stable and efficient production of silicon in three-phase submerged arc furnaces relies on precise heat-control of the reaction zone. As the heat is generated by the electric currents flowing through each of the three electrodes, the heat-control translates to controlling the electric power in each electrode. To determine the electrode powers, the electrode voltages must be determined through measurements. Typically, the electrode voltages are measured relative to the neutral point of the electrodes' notional star connection using the so-called Bøckman method. The Bøckman method relies on three measurement leads outside the furnace, each connected to the furnace bottom, to cancel voltages induced by the large magnetic fields in the vicinity of the furnace. The two main sources of error associated with the Bøckman method are induction and neutral-point drift. For an idealized and symmetric furnace, the induced voltages in three symmetrically placed leads cancel, and the true neutral point of the voltage will be at the furnace centre. However, during operation the induced voltages will change with the dynamically changing current paths inside the furnace, and the neutral point will dynamically drift, leading to errors in the measured voltages.
To study these effects, we have developed Finite Element Method (FEM) simulation models of industry-scale three-phase silicon furnaces. The models are implemented in COMSOL Multiphysics and are used to calculate the electromagnetic fields within the furnace (including the electrodes, linings and steel casing) as well as the induced voltages in leads placed around the furnace, mimicking the Bøckman measurement system.

Through simulations we have investigated how asymmetric furnace conditions lead to neutral point drift. Furthermore, we have estimated the contribution to the measured neutral point drift from an asymmetric or poorly calibrated Bøckman system. The model results have been considered together with industrial measurements of neutral point drift.

1. INTRODUCTION

Production of Silicon requires vast amounts of energy to heat up and transform quartz into a metal alloy. The production process takes place in submerged arc furnaces (SAFs), where the necessary energy is provided by electric current through three large electrodes. In a stepwise process, the solid quartz (SiO_2) is transformed into liquid silicon (Si) of varying grade. The Si-yield and production of by-products are highly dependent on temperature. Thus, to run an optimal Si-production the heat balance within the furnace must be properly controlled, to ensure the desired temperatures (Westly, 1974; Westly, 1975; Stewart, 1980; Schei, Tuset and Tveit, 1998).

Efficient control of the heat balance in the furnace hearth requires a good estimate of the electric power provided through each of the three electrodes, which in turn requires good measurements of the electrode currents and the voltage drop over the electrodes. The electrode currents are most readily available and can be measured outside the furnace itself. As for the voltage drops, there is no single accessible neutral point, for which to measure the potential difference. The three electrode currents will connect through a notional star connection at some point in the furnace hearth (Stewart, 1980; Barker and Stewart, 1980; Stewart and Barker, 1980; Gerritsen, Tracy and Saber, 2015). For a perfectly symmetric furnace, the electric potential will be zero at the vertical centre axis. A common way to estimate the voltage drop is the so-called Bøckman measurement system which applies three leads between a common centre point at the bottom of the furnace and the top of each electrode (Bøckman, 1973a; Bøckman, 1973b). The use of electric leads around the furnace is prone to measurement errors due to induced voltages from the strong magnetic fields surrounding the furnace. However, the use of three leads allows to cancel out induction errors, due to the three-part rotational symmetry of the three-phase electrode currents.

For precise measurements, two main obstacles occur. Firstly, setting up three leads perfectly symmetric around the furnace is in practice very difficult. Secondly, the neutral point inside the furnace is not fixed, as it will vary with dynamical changes to the inner geometry and material properties of the furnace. It will also vary with electrode movements and arcing. This effect is referred to as *neutral point drift* (Stewart and Barker, 1980; Barker 1980). An asymmetric set-up of the leads will affect the inductive cancellation by skewing the contribution to each lead. This effect can be counteracted by having an adjustable resistance for each lead, which can be tuned to achieve balance between the three leads. Usually, this is a procedure that takes place at a single point in time at the start of the furnace's lifespan. When tuning the resistance network, it is assumed that the neutral point is well defined in the centre of the furnace. Thus, if due to material imbalance, the true neutral point is significantly off centre, the tuning of the resistances will be affected (Sparta, Risingård, Thisted, 2024a; Sparta, Risingård, Thisted, 2024b).

In this publication, a finite element model of a three-phase submerged arc furnace is presented. The model builds on previous research of both inner conditions as well as models of the Bøckman system (Herland, Sparta and Halvorsen, 2018; Sparta, Risinggård and Thisted, 2024a; Sparta, Risinggård and Thisted, 2024b). The novelty of this work is in the investigation of simulation cases with quantitively different asymmetries, to investigate the impact on neutral point drift and thereby the effect on the Bøckman compensation. The study is partly motivated by industrial measurement campaigns that observed neutral point drift, the key findings of which are briefly presented in this publication.

2. Furnace model and simulations

A furnace model has been simulated using the *Magnetic and Electric Fields* interface in *COMSOL Multiphysics* (COMSOL, 2025). Here, Maxwell's equations were solved for the electric potential and magnetic vector potential in the frequency domain. The model is a continuation of previous modelling work of three-phase furnaces, and further details about the implementation can be found in (Herland, Sparta and Halvorsen, 2018; Sparta *et al.*, 2021; Sparta *et al.*, 2022; Sparta, Risinggård and Thisted, 2024a; Sparta, Risinggård and Thisted, 2024b). The electromagnetic fields are governed by Maxwell's equations, which in the frequency domain can be written as (assuming no accumulation of charge)

$$i\omega\mathbf{B} + \mathrm{curl}\,\mathbf{E} = \mathbf{0}, \quad [1]$$
$$i\omega\mathbf{D} - \mathrm{curl}\,\mathbf{H} = -\mathbf{J}, \quad [2]$$
$$\mathrm{div}\,\mathbf{B} = 0, \quad [3]$$
$$\mathrm{div}\,\mathbf{E} = 0. \quad [4]$$

Each of the vector fields represent the complex amplitude of the respective fields, where **B** is the magnetic induction, **H** is the magnetic field, **E** is the electric field, **D** is the electric displacement and **J** is the electric current density. In addition to Maxwell's equations, Ohms law, $\boldsymbol{J} = \sigma \boldsymbol{E}$, is also included in the model formulation. The model is solved in terms of the scalar electric potential V and magnetic vector potential **A**, defined as $\mathbf{B} = \mathbf{curl}\ \mathbf{A}$ and grad $V = -\mathbf{E} + i\omega\mathbf{A}$.

The furnace model includes a steel shell, steel roof, carbon lining, alumina refractories and electrodes. In addition, a large region of non-conducting air surrounds the domain to secure a well posed boundary condition for the magnetic field. The mathematical model is completed with introducing appropriate boundary conditions for **A** and V. An electric potential is fixed on top of each of the electrodes, while magnetic insulation is assumed for the remaining outer boundary of the computational domain. In addition, the model utilizes the impedance boundary conditions to remove the computationally costly steel shell domain from the computations (Herland, Sparta and Halvorsen, 2018; Fromreide *et al.* 2023). The computational domain is discretized using mainly tetrahedral mesh elements, with refined rectangular boundary elements at the boundaries of very well conducting domains, such as the electrodes and metal alloy. The Bøckman leads which are located outside the furnace are meshed using edge-elements.

The interior of the furnace is divided into zones with bulk properties to represent the distribution of material and heat zones of a real industrial furnace. The charge material is divided into three zones, a cold top layer, a middle outer reaction zone and an inner high-temperature reaction zone. Each of the vertically stacked layers are further divided in three sections, so that the conditions around each individual electrode can be adjusted. At the bottom of each electrode a crater with surrounding crater walls is defined. The model is fully parameterized and further includes the possibility of side arcs (electrode – crater wall) and a bottom arc (electrode – alloy). Side-arcs are included if the distance between the electrode and crater wall is 15 cm or less and is approximated by cylindrical resistive domains. The same is true for the bottom arc for the distance between the electrode and alloy. However, for the simulations treated in this publication, no bottom arcs are included as only higher electrode positions are considered. A sketch of the different material zones can be seen in Figure 1.

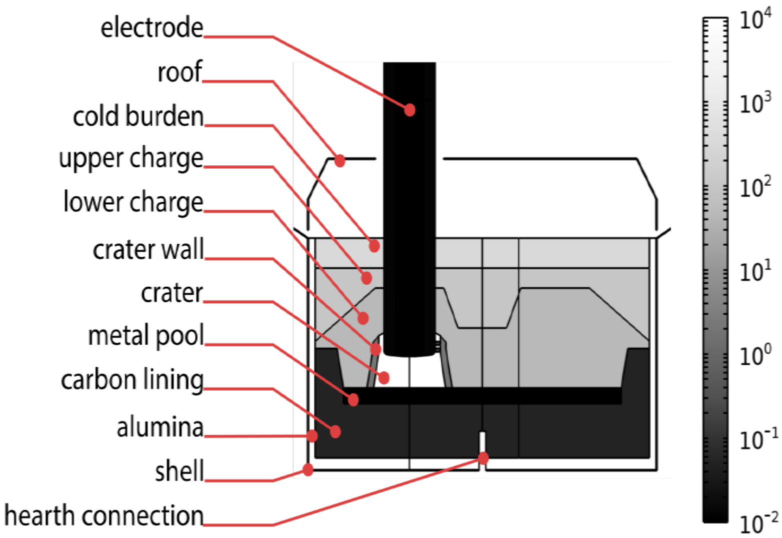

Figure 1: Schematic representation of model geometry and material zones.
The color bar shows the resistivity of the materials inside the furnace in mΩ·m.

2.1 Simulation cases

Surrounding the furnace model a network of possible Bøckman leads is placed. In general, any three symmetrically (120° separation) placed leads will give perfect cancellation. A perfect symmetric placement is difficult to obtain in practice, the simulations carried out in this work considered asymmetric leads (Sparta, Risinggård and Thisted, 2024a; Sparta, Risinggård and Thisted, 2024b). Three leads have been chosen, with angular separations of 100°, 150° and 110°. The angular position relative to the electrodes is shown in the 2D furnace sketch in Figure 2. This work only considers angular displacement of the leads, keeping the radial distance from the furnace constant for each lead. In reality, the displacement will generally vary in both the angular and radial direction as a function of the furnace height.

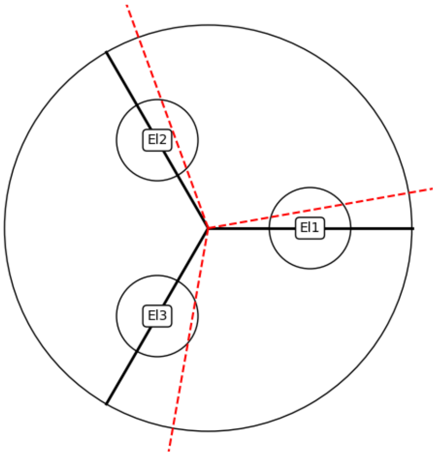

Figure 2: Placement of asymmetric Bøckman leads

A default case has been defined where the furnace is completely symmetric with each electrode in the same position. Then, more cases have been chosen by introducing an unbalance in the resistivities of the inner material zone surrounding the three electrodes. Due to the geometry of the model and the typical value range (20-80 mΩ·m) for the bulk resistivity of these regions, they have the single most impact on the current distribution (Fromreide *et al.*, 2021). For each simulation case, the electrode resistances are kept constant by allowing the electrodes to shift down or up to account for the change in material resistivity. The bulk resistivity in each inner reaction zone can be either decreased, increased or be kept constant. Thus, there are a total of $3^3 = 27$ qualitatively different combinations to explore. However, due to rotational symmetry (e.g. (0 - -) can be rotated to give (– 0 –) and so forth) and the fact that some combinations will be scaled versions of others (e.g. (- - 0) and (- - +) will give the same asymmetry), only four asymmetric settings are needed to span the set of possibilities and get an estimate for how different variations will affect the model. The full factorial design with the four selected cases is shown in Table 1.

The default setting for the bulk resistivity of the inner charge zone has been set to 47 mΩ·m. The asymmetries have then been introduced by either keeping this value approximately constant, increasing it to approximately 70 mΩ·m or lowered to approximately 30 mΩ·m for each individual region between and surrounding the electrodes. To get constant electrode resistances within reasonable electrode positions, some adjustments have been made to the different cases. The value used for each case is defined in Table 2, together with electrode tip positions which are adjusted as a response to the chosen bulk resistivities.

Table 1: Factorial design of the 27 qualitatively different combinations of variations in material resistivity. 0 denotes a medium value, - a low value and + a high value. The five selected simulation cases are indicated.

#	Value	#	Value	#	Value
1	− − −	10	0 − −	19	+ − −
2	− − 0	11	0 − 0	20	+ − 0
3 (D)	− − +	12	0 − +	21 (A)	+ − +
4	− 0 −	13	0 0 −	22 (C)	+ 0 −
5	− 0 0	14 (Sym)	0 0 0	23	+ 0 0
6 (B)	− 0 +	15	0 0 +	24	+ 0 +
7	− + −	16	0 + −	25	+ + −
8	− + 0	17	0 + 0	26	+ + 0
9	− + +	18	0 + +	27	+ + +

Table 2: Parameter settings for the varying parameters for the five simulation cases.

Parameter	Sym.	A	B	C	D
Electrode 1 tip position (m)	0.80	0.61	0.82	0.73	0.86
Electrode 2 tip position (m)	0.80	0.94	0.87	0.78	1.01
Electrode 3 tip position (m)	0.80	0.80	0.57	0.95	0.76
Resistivity inner zone 1-2 (mΩ·m)	47	70	28	72	40
Resistivity inner zone 2-3 (mΩ·m)	47	31	50	50	40
Resistivity inner zone 3-1 (mΩ·m)	47	71	72	40	70

3. Results

Each of the simulations defined in Table 2 has been solved in COMSOL Multiphysics. From the calculations, the induced voltage in the defined asymmetric Bøckman leads has been extracted as complex amplitudes together with the calculated electric potential at the point of access (PA) at the furnace bottom. Given the amplitudes for the individual leads, the resistances needed to compensate for neutral point drift is found by solving two equations, on for the real part and one for the imaginary part of the three vectors. Thus, one of the leads resistances are kept constant while two are scaled. The value of the two scalars is found numerically using the least square fit algorithm in the python library *scipy* (Virtanen *et al.*, 2020), accounting for small numerical errors arising from the FEM simulations. Figure 3 shows

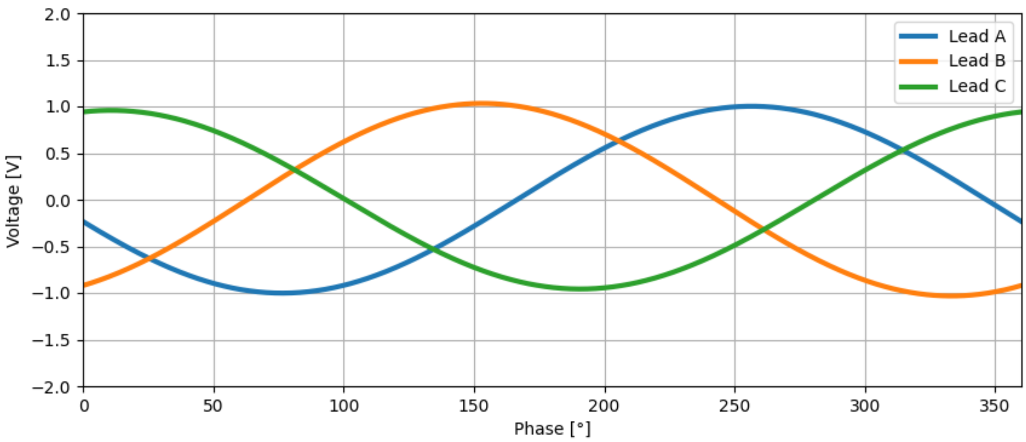

Figure 3: Induced voltage in the three Bøckman leads for the symmetric furnace. The values have been scaled by the voltage amplitude measured in Lead A.

the induced voltage in each of the three Bøckman leads for the symmetric case. For confidentiality, the scales have been adjusted, but the relative trends are kept in all the subsequent plots by scaling with the same value The results are illustrated as curves over one phase. The value for each lead is then added together with the contribution from the voltage at PA to find the measured Bøckman potential, which for a perfect symmetric Bøckman measurement should be zero. The result is shown in Figure 4 together with the measured potential at PA and the compensated Bøckman measurement. As the figure shows, the uncompensated measured neutral point is different from the true voltage at PA due to the asymmetric Bøckman set up. However, the scaling of two of the lead resistances perfectly compensates the measured value.

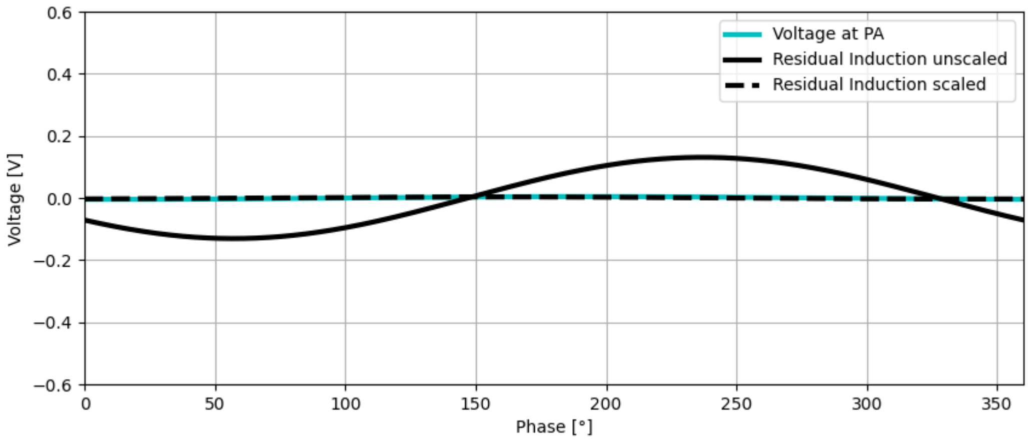

Figure 4: Measured voltage at connection point at the furnace bottom (PA), unscaled neutral point measured from the leads and scaled induction. The values have been scaled by the voltage amplitude of measured in Lead A.

Figure 5 shows the results from the four asymmetric simulation cases. There are notable differences between the cases, both in terms of magnitude and phase shift. Further, it is seen that the simple tuning of resistances does not fully compensate for the neutral point drift in any of the cases. For the uncompensated cases the magnitude of the simulated measured Bøckman voltage varies between 1.13 and 2.61 times the "true" zero potential measured at the furnace bottom (PA). Likewise, the phase error varies between 4° and 42°. Similarly, for the compensated leads, the magnitudes vary between 1.20 and 1.60 times the measured voltage at PA, with phase errors in the range 0° to 24°. The overestimation of the voltage magnitude and the variation in phase is in line with previous results in (Sparta, Risinggård and Thisted, 2024a; Sparta, Risinggård and Thisted, 2024b). The results are summarized in Table 3, which states the offset in terms of both the relative amplitude and absolute phase for each case. The results show that a single calibration of the resistance network is not sufficient for proper compensation. However, apart from case A, which showed a good agreement between the uncompensated Bøckman voltage and the voltage at PA, the compensation works in a positive way as it reduces the offset. It is a notable significant positive effect on the phase shift, which is important for furnace control.

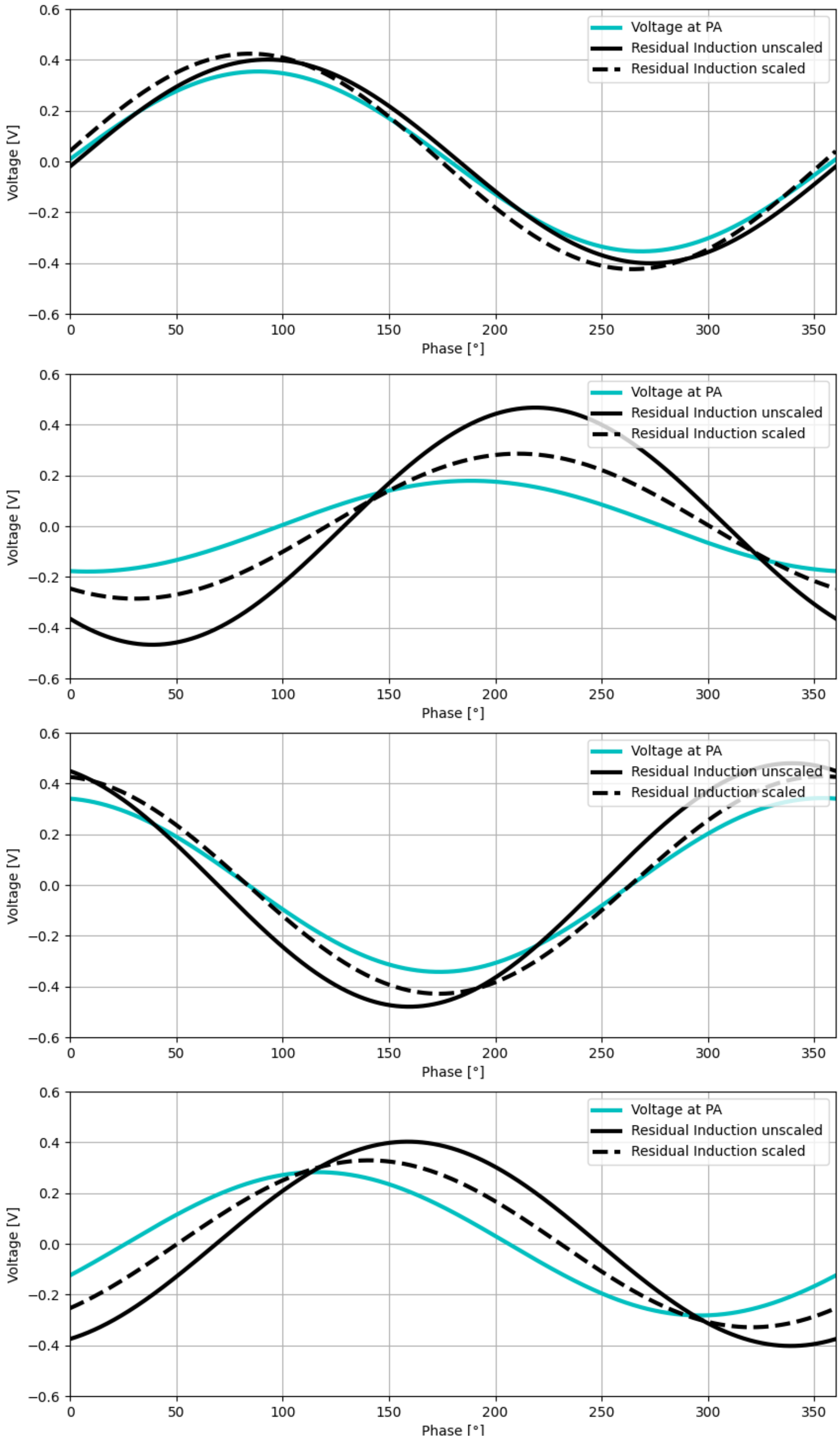

Figure 5: Measured voltage at PA, unscaled and scaled neutral point measured from the leads. Cases A, B, C and D (from top to bottom). The values have been scaled by the voltage amplitude measured in Lead A.

Table 3: Deviation of the "measured" neutral point voltage and the voltage at PA in terms of the relative amplitude (first row) and phase angle (last row) for the four asymmetric cases. U and C denote uncompensated and compensated, respectively.

	A		**B**		**C**		**D**	
	U	C	U	C	U	C	U	C
$\left\|\frac{\|V_{PA}\| - \|V_0\|}{\|V_{PA}\|}\right\|$	0.13	0.19	1.6	0.60	0.40	0.25	0.42	0.16
$\angle V_{PA} - \angle V_0$	-4.1°	4.5°	-30.4°	-22.3°	14.3°	0.28°	-42.6°	-24.3°

The numerical studies have partly been motivated by measurement campaigns performed at an industrial silicon furnace. The furnace is approximately 30 MW and has a geometry and dimensions which are reasonably close to those used in the numerical models. The furnace was equipped with sensors capable of measuring the electrode voltages at a high frequency, enabling a good resolution of one phase period (50 Hz). Figure 6 shows a 20-minute data window from one measurement campaign. The magnitude of the potential is omitted for confidentiality, while relative trends and phase errors are presented. Preliminary results from this measurement campaign have previously been published in a master's thesis (Monsen, 2025), where more information about the measurements set up can be found. As the figure shows, the potential circles around the neutral point with some notable distinct drifts in the region 250°- 360°. The figure highlights that neutral point drift can cause significant errors in measured electrode voltages.

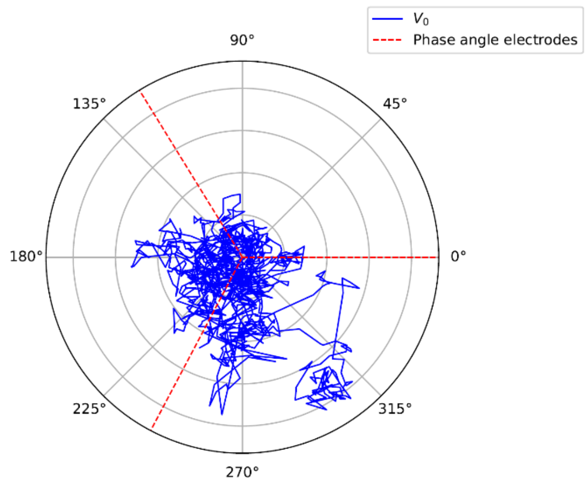

Figure 6: Measured neutral point drift over a 20-minute period from an industrial silicon furnace. The magnitude of the voltage has been omitted for confidentiality; relative trends are preserved.

5. CONCLUSIONS

Measurements of electrode voltages in an industrial silicon furnace indicate that neutral-point drift is significant as a source of error in the electrode voltage. it has been shown how significant drift in the neutral point phase occur over a short time-period during normal operation. The error arising from neutral point drift has a larger impact compared to previous estimates of induction-related errors. Contributions to the neutral-point measurement from asymmetries in the placement of the Bøckman leads have been estimated using finite-element simulations. It has been shown that different asymmetries give variations in the measured off-set and that a single calibration is insufficient for proper compensation. The simulations highlight the critical role of practical procedures for compensating for geometric asymmetries in the voltage measurement system.

In this study, the compensation was based on a fully symmetric furnace, and the simulation cases were established assuming constant electrode resistance. Both assumptions represent idealized operating conditions. Future work will extend the analysis to investigate Bøckman lead compensation in asymmetric furnace configurations and to employ constant electrode current as the governing condition, thereby providing a more realistic representation of industrial furnace operation.

6. ACKNOWLEDGEMENTS

This work was supported by the project "Submerged-arc furnaces: Improved electrical conditions for increased energy efficiency and decarbonization" (SAPPHIRE) funded by the Research Council of Norway (grant number 358034) and the Norwegian Ferroalloy Producers' Research Association (FFF) with the member companies Elkem ASA, Eramet Norway AS, Finnfjord AS, and Wacker Chemicals Norway AS.

7. REFERENCES

Barker, I.J. 1980. *IFAC Proc. Vol.*, vol. 13, pp. 611–21, https://doi.org/10.1016/s1474-6670(17)64768-2.

Barker, I.J. and Stewart, A.B. 1980 *J. South. Afr. Inst. Min. Metall.*, 1980, vol. 80, pp. 123–28, http://www.saimm.org.za/Journal/v080n03p123.pdf.

Bøckman, O.C. 1973. NO126288B, Jan. 1973, https://patents.google.com/patent/NO126288B/en.

Bøckman, O.C. 1973. US3757021, Sep. 1973, https://patents.google.com/patent/US3757021/en.

COMSOL Inc.: *AC/DC Module User's Guide*, 2025.

Fromreide, M., Gomez, D., Halvorsen, S. A., Herland, E. V. and Salgado, P. 2021. Reduced 2D/1D mathematical models for analyzing inductive effects in submerged arc furnaces. Applied Mathematical Modelling, 98,59-70.

Fromreide, M, Gomez, D., Halvorsen, S. A. and Salgado, P. 2023 Induced currents in the lining and steel shell of submerged arc furnaces. Journal of Sustainable Metallurgy 9.1: 375-385.

Gerritsen, T., Tracy, P. and Saber, F. 2015. in *Proc. INFACON XIV*, International Committee on Ferro-Alloys, Kyiv, Ukraine, 2015, pp. 338–48, https://www.pyrometallurgy.co.za/InfaconXIV/338-Gerritsen.pdf.

Herland, E.V., Sparta, M. and Halvorsen, S.A. 2018 *J. South. Afr. Inst. Min. Metall.*, vol. 118, pp. 607–18, https://doi.org/10.17159/2411-9717/2018/v118n6a8.

Monsen, I. 2025, Circuit Modelling of Submerged Arc Furnaces and Their Power Supply Systems, M.Sc. thesis, University of Oslo

Schei, A., Tuset, J.K. and Tveit, H. 1998, Production of High Silicon Alloys, Tapir forlag, Trondheim,

Sparta, M., Fromreide, M. Risinggård, V.K. Halvorsen, S.A. 2022 in *Proc. Silicon Chem. Sol. Industry XVI*, SSRN Electronic Journal, Trondheim, 2022, https://doi.org/10.2139/ssrn.4118651.

Sparta, M., Risinggård, V.K. and Thisted U. 2024 in *Proc. Silicon Chem. Sol. Industry XVII*, Social Science Research Network, Trondheim, Norway, 2024, https://doi.org/10.2139/ssrn.4942623.

Sparta, M., Risinggård, V.K. and Thisted U. 2024. NORCE Research AS, Kristiansand, Norway, 2024.

Sparta, M., Varagnolo, D. Stråbø, K., Halvorsen, S.A., Herland, E.V. and Martens, H. 2021. *Metall. Mat. Trans. B*, vol. 52, pp. 1267–78, https://doi.org/10.1007/s11663-021-02089-7.

Stewart, A.B. 1980. PhD Thesis, University of Cape Town, 1980, http://hdl.handle.net/11427/14048.

Stewart, A.B. and Barker, I.J. 1980. in *Proc. INFACON II*, International Committee on Ferro-Alloys, Lausanne, Switzerland, 1980, pp. 71–82, https://www.pyrometallurgy.co.za/InfaconII/071-Stewart.pdf.

Pauli Virtanen, Ralf Gommers, Travis E. Oliphant, Matt Haberland, Tyler Reddy, David Cournapeau, Evgeni Burovski, Pearu Peterson, Warren Weckesser, Jonathan Bright, Stéfan J. van der Walt, Matthew Brett, Joshua Wilson, K. Jarrod Millman, Nikolay Mayorov, Andrew R. J. Nelson, Eric Jones, Robert Kern, Eric Larson, CJ Carey, İlhan Polat, Yu Feng, Eric W. Moore, Jake VanderPlas, Denis Laxalde, Josef Perktold, Robert Cimrman, Ian Henriksen, E.A. Quintero, Charles R Harris, Anne M. Archibald, Antônio H. Ribeiro, Fabian Pedregosa, Paul van Mulbregt, and SciPy 1.0 Contributors. 2020 SciPy 1.0: Fundamental

Algorithms for Scientific Computing in Python. Nature Methods, 17(3), 261-272. DOI: 10.1038/s41592 019-0686-2.
Westly, J. 1974. in *Proc. INFACON I*, International Committee on Ferro-Alloys, Johannesburg, South Africa, pp. 121–27, https://www.pyrometallurgy.co.za/InfaconI/121-Westly.pdf.
Westly, J. 1975. in *Proc. Elec. Furn. Conf.*, Iron & Steel Society, pp. 47–53.

Mads Fromreide
Senior Researcher, NORCE Research AS
Mads Fromreide holds a PhD in Applied Mathematics from the University of Santiago de Compostela. He has worked at NORCE for over a decade, mainly working on modelling towards the metallurgical industry.